



Charging and coagulation of radioactive and nonradioactive particles

Y.-H. Kim et al.

This discussion paper is/has been under review for the journal Atmospheric Chemistry and Physics (ACP). Please refer to the corresponding final paper in ACP if available.

Charging and coagulation of radioactive and nonradioactive particles in the atmosphere

Y.-H. Kim¹, S. Yiacoumi¹, A. Nenes^{2,3}, and C. Tsouris^{1,4}

¹School of Civil and Environmental Engineering, Georgia Institute of Technology, Atlanta, Georgia, 30332-0373, USA

²School of Earth and Atmospheric Sciences, Georgia Institute of Technology, Atlanta, Georgia, 30332-0340, USA

³School of Chemical and Biomolecular Engineering, Georgia Institute of Technology, Atlanta, Georgia, 30332-0100, USA

⁴Oak Ridge National Laboratory, Oak Ridge, Tennessee, 37831-6181, USA

Received: 4 August 2015 – Accepted: 6 August 2015 – Published: 3 September 2015

Correspondence to: C. Tsouris (tsourisc@ornl.gov)

Published by Copernicus Publications on behalf of the European Geosciences Union.

Title Page

Abstract

Introduction

Conclusions

References

Tables

Figures



Back

Close

Full Screen / Esc

Printer-friendly Version

Interactive Discussion



Abstract

Charging and coagulation influence one another and impact the particle charge and size distributions in the atmosphere. However, few investigations to date have focused on the coagulation kinetics of atmospheric particles accumulating charge. This study presents three approaches to include mutual effects of charging and coagulation on the microphysical evolution of atmospheric particles such as radioactive particles. The first approach employs ion balance, charge balance, and a bivariate population balance model (PBM) to comprehensively calculate both charge accumulation and coagulation rates of particles. The second approach involves a much simpler description of charging, and uses a monivariate PBM and subsequent effects of charge on particle coagulation. The third approach is further simplified assuming that particles instantaneously reach their steady-state charge distributions. It is found that compared to the other two approaches, the first approach can accurately predict time-dependent changes in the size and charge distributions of particles over a wide size range covering from the free molecule to continuum regimes. The other two approaches can reliably predict both charge accumulation and coagulation rates for particles larger than about 40 nm and atmospherically relevant conditions. These approaches are applied to investigate coagulation kinetics of particles accumulating charge in a radioactive neutralizer, the urban atmosphere, and a radioactive plume. Limitations of the approaches are discussed.

1 Introduction

Atmospheric particles play an important role in airborne transport of contaminants, such as radionuclides. Contaminants emitted from anthropogenic sources (e.g., nuclear plant accidents) can be captured by background aerosols and then are transported together with pre-existing particles. Contaminant-laden particles can be deposited onto the ground by dry and wet deposition (primary contamination) and subsequently resuspended by wind or heat-driven convection and moved to other areas

Charging and coagulation of radioactive and nonradioactive particles

Y.-H. Kim et al.

Title Page

Abstract

Introduction

Conclusions

References

Tables

Figures

◀

▶

◀

▶

Back

Close

Full Screen / Esc

Printer-friendly Version

Interactive Discussion



Charging and coagulation of radioactive and nonradioactive particles

Y.-H. Kim et al.

Title Page

Abstract

Introduction

Conclusions

References

Tables

Figures

◀

▶

◀

▶

Back

Close

Full Screen / Esc

Printer-friendly Version

Interactive Discussion

(secondary contamination). Due to atmospheric dispersion, radioactive particles (e.g., ^{137}Cs) released during the Fukushima accident were sampled in situ 150 km away from the emission site (Yamauchi et al., 2012). Similar dispersion patterns of radioactive particles were observed after the Chernobyl accident (Yoshenko et al., 2006a, b). Accurate understanding of the behavior of atmospheric particles is necessary to precisely predict transport of contaminants (especially long-lived ones, such as ^{137}Cs), as well as their potential environmental impacts.

The behavior of atmospheric particles is driven by such properties as charge and size that can affect particle deposition and other microphysical processes (Fuchs, 1989; Pruppacher and Klett, 1997). Atmospheric particles can acquire charge via self-charging and diffusion charging; radioactive particles can be charged through these two charging mechanisms (Greenfield, 1956; Yeh et al., 1976; Clement and Harrison, 1992; Clement et al., 1995; Gensdarmes et al., 2001; Walker et al., 2010; Kweon et al., 2013; Kim et al., 2014, 2015) while natural atmospheric particles are typically charged by diffusion charging (Hoppel, 1985; Yair and Levin, 1989; Renard et al., 2013). Particle charging can modify not only the charge but also the size distribution because charge on the particles generates electrostatic surface interactions that facilitate or hinder particle coagulation (Fuchs, 1989; Tsouris et al., 1995; Chin et al., 1998). Coagulation of atmospheric particles can influence their charging because the particle size distribution can highly affect the time-evolution of ion concentrations (Yair and Levin, 1989). Also, particle coagulation can result in charge neutralization or accumulation on atmospheric particles (Alonso et al., 1998). Particle charging and coagulation can mutually affect each other and simultaneously affect both charge and size distributions in the atmosphere.

Theoretical and experimental investigations have been performed to examine the charging of radioactive particles and background aerosols in the atmosphere. However, the effects of coagulation of particles on the charge distribution have been frequently neglected by assuming that the size distribution is constant while they are charged (Greenfield, 1956; Hoppel, 1985; Yair and Levin, 1989). The assumption may be valid

Charging and coagulation of radioactive and nonradioactive particles

Y.-H. Kim et al.

Title Page

Abstract

Introduction

Conclusions

References

Tables

Figures



Back

Close

Full Screen / Esc

Printer-friendly Version

Interactive Discussion



if the particle concentration is low or the steady-state charge distribution is instantaneously attained (Hoppel, 1985; Renard et al., 2013; Kim et al., 2015). If the timescale for particle charging is longer than that for particle coagulation, the assumption may no longer be valid (Yair and Levin, 1989). Also, the effects of charging on the particle size distribution are frequently neglected in aerosol transport models involving microphysics of atmospheric particles. A possible reason for neglecting the charging effects may be that the steady-state mean charge of atmospheric particles rarely may affect their coagulation rates (Seinfeld and Pandis, 2006). However, neglecting electrostatic particle-particle interactions may increase uncertainty of prediction results if particles can acquire multiple elementary charges (e.g., radioactive particles). The simplified assumption of omitting electrostatic particle interactions may create uncertainty in transport predictions of radioactive particles. Hence, it may be necessary to take into account the mutual effects of particle charging and coagulation processes in predicting the behavior of atmospheric particles carrying radioactive contaminants.

Previous attempts to consider charging effects include Oron and Seinfeld (1989a, b), who developed sectional approaches to simultaneously predict the behavior of charged and uncharged atmospheric particles. Laakso et al. (2002) developed a general dynamic equation, including charging and coagulation kinetics of atmospheric particles. However, the validity of these approaches was not evaluated using analytical solutions. Alonso (1999) and Alonso et al. (1998) developed analytical and numerical approaches to estimate time-dependent changes in the size distributions of singly charged and neutral particles; thus, these approaches cannot be used to investigate the coagulation kinetics of particles acquiring multiple elementary charges. Also, none of these approaches considered self-charging; therefore, the aforementioned approaches may be subject to error when they are used to simulate atmospheric dispersion of radioactive plumes.

Our study presents three approaches to simultaneously predict time-dependent changes of the charge and size distributions of radioactive and nonradioactive parti-

cles over a wide size range. Development, validity, application, and limitations of these approaches are discussed.

2 Model development

2.1 Ion balance model

5 Many atmospheric processes can generate and remove ions in air. Typical ion sources in the atmosphere involve natural and artificial radioactivity, as well as cosmic rays. Ions are generally removed by ion-ion recombination and ion-particle attachment. Changes in ion concentrations by these processes can be given by (Kim et al., 2015):

$$\frac{dn_+}{dt} = -n_+ \sum_k \sum_j \beta_{k,j}^+ N_{k,j} - \alpha_{rc} n_+ n_- + q, \quad (1)$$

$$10 \frac{dn_-}{dt} = -n_- \sum_k \sum_j \beta_{k,j}^- N_{k,j} - \alpha_{rc} n_+ n_- + q + q_e, \quad (2)$$

where n_{\pm} refers to the number concentrations of positive or negative ions, the indices k and j represent the size and number of elementary charges of particles, respectively, $\beta_{k,j}^{\pm}$ is the attachment coefficient between a particle and an ion, $N_{k,j}$ is the number concentration of particles, α_{rc} is the recombination coefficient of ions, and t is time. The first two terms of the right-hand-side (RHS) of Eqs. (1) and (2) represent the loss rate of ions due to ion-particle attachment and ion-ion recombination, respectively. The third term denotes the production rate of ion pairs, q :

$$q = q_b + q_l, \quad (3)$$

20 where q_b is the ion production rate by cosmic rays and natural radioactivity, and q_l is the ion production rate by radionuclides released by nuclear events. Electrons released by

radioactive decay are taken into account via the last term of Eq. (2). Changes in the ion concentrations may affect the electrical conductivity of the atmosphere, σ_{air} (Harrison and Carslaw, 2003):

$$\sigma_{\text{air}} = e (\mu_+ n_+ + \mu_- n_-), \quad (4)$$

where e is the elementary charge and μ_{\pm} is the mobility of positive or negative ions. In Eq. (4), the terms in the parentheses of the RHS represent polar air conductivities.

2.2 Charge balance models

Self-charging refers to charge accumulation caused by radioactive decay which typically leads to emission of electrons from particle surfaces. Diffusion charging is attributed to diffusion of ions from the surrounding atmosphere onto the surface of particles. Self-charging generally accumulates positive charge on the surface of particles, while diffusion charging adds both positive and negative charges, indicating that the charging mechanisms can compete with one another. For radioactive particles involved in beta decay, time-dependent changes in their charge distributions due to competition of the charging mechanisms can be expressed by (Clement and Harrison, 1992; Kim et al., 2015):

$$\begin{aligned} \frac{dN_{k,j}}{dt} = & \eta_{k,j-1} N_{k,j-1} - \eta_{k,j} N_{k,j} + \beta_{k,j-1}^+ n_+ N_{k,j-1} - \beta_{k,j}^+ n_+ N_{k,j} \\ & + \beta_{k,j+1}^- n_- N_{k,j+1} - \beta_{k,j}^- n_- N_{k,j}, \end{aligned} \quad (5)$$

where η is the decay rate of the radioactive particles. In Eq. (5), self-charging is represented by terms that include η , while diffusion charging is represented by terms with $\beta_{k,j}^{\pm}$. If the terms for self-charging are removed, Eq. (5) becomes identical to the charge balance model presented by Renard et al. (2013) who predicted electrification phenomena of aerosols in the real atmosphere. The mean value of the particle charge

Charging and coagulation of radioactive and nonradioactive particles

Y.-H. Kim et al.

Title Page

Abstract

Introduction

Conclusions

References

Tables

Figures

◀

▶

◀

▶

Back

Close

Full Screen / Esc

Printer-friendly Version

Interactive Discussion



distributions can be given by:

$$\frac{dJ_k}{dt} = \frac{d}{dt} \left(\frac{\sum j N_{kj}}{\sum N_{kj}} \right). \quad (6)$$

The mean charge J of the radioactive particles of size k can also be approximated using a simple charge balance equation (Kim et al., 2015):

$$\frac{dJ_k}{dt} = \eta_k + \beta_{k,J}^+ n_+ - \beta_{k,J}^- n_-. \quad (7)$$

Similarly to Eq. (5), the mean charge accumulation rate of the radioactive particles (Eq. 7) depends on the competition between self- and diffusion charging. Equations (5) and (7) indicate that the net charge of beta-emitting radioactive particles converges to a steady state where self-charging balances diffusion charging. The timescale, τ , needed to reach a steady state can be given by (Clement and Harrison, 1992):

$$\tau = \frac{1}{\beta^- n_-}. \quad (8)$$

At steady state, the mean charge of the radioactive particles can be approximated using (Clement et al., 1995):

$$J_k = \begin{cases} y - \left(\frac{y(X-1)}{\exp(2\lambda y)-1} \right) & \lambda y > 0.22 \\ y + \frac{X-1}{2\lambda} & \lambda y \leq 0.22 \end{cases}, \quad (9)$$

with $\lambda = \frac{e^2}{8\pi\epsilon_0\epsilon_r r_k k_B T}$, $y = \frac{\epsilon_0 \eta_k}{e\mu_- n_0}$, $n_0 = \sqrt{\frac{q}{\alpha}}$, $X = \frac{\mu_+ n_+}{\mu_- n_-}$, where ϵ_0 is the vacuum permittivity, ϵ is the dielectric constant of the air, r is the radius of particles, k_B is the Boltzmann constant, T is the temperature, n_0 is the mean ion concentration, and I is the ionization rate coefficient of beta-emitting radionuclides. Equation (9) suggests that the steady-state mean charge of beta-emitting radioactive particles is highly influenced by their

Charging and coagulation of radioactive and nonradioactive particles

Y.-H. Kim et al.

Title Page

Abstract

Introduction

Conclusions

References

Tables

Figures

◀

▶

◀

▶

Back

Close

Full Screen / Esc

Printer-friendly Version

Interactive Discussion



size and decay rates, as well as the concentrations and mobilities of ions in air. The second term of the RHS of Eq. (9, second row) represents charge accumulated only by diffusion charging; thus, it can be used to approximate the steady-state mean charge of nonradioactive particles, such as background aerosols that are externally mixed with radionuclides.

2.3 Population balance models

2.3.1 Bivariate population balance model

A bivariate population balance model, expressed in terms of particle volume x and charge j , can be used to predict effects of coagulation on time-dependent changes in the particle size and charge distributions. In the bivariate population balance model, the time-evolution of the number densities of charged and uncharged particles, n , due to coagulation, can be given by (Zebel, 1958; Oron and Seinfeld, 1989a, b):

$$\frac{\partial n(x, j)}{\partial t} = \frac{1}{2} \sum_{j'=-\infty}^{\infty} \int_0^x F_{j', j-j'}(x', x-x') n(x', j') n(x-x', j-j') dx' - \sum_{j'=-\infty}^{\infty} \int_0^{\infty} F_{j, j'}(x, x') n(x, j) n(x', j') dx' \quad (10)$$

where F is the coagulation frequency, which can be obtained by multiplying the collision frequency and the collision efficiency. The two terms on the RHS of Eq. (10) represent the production and loss rates of charged and uncharged particles by coagulation, respectively. A numerical solution of Eq. (10) can be obtained through the discretization of the integral terms, respectively (Oron and Seinfeld, 1989a, b). Vanni (2000) tested several sectional approaches and showed that the approach of Kumar and Ramkrishna (1996) is simpler and more accurate than other tested approaches, and also preserves

Charging and coagulation of radioactive and nonradioactive particles

Y.-H. Kim et al.

Title Page

Abstract

Introduction

Conclusions

References

Tables

Figures

◀

▶

◀

▶

Back

Close

Full Screen / Esc

Printer-friendly Version

Interactive Discussion



mass and number of particles. Thus, the sectional approach of Kumar and Ramkrishna (1996) was used in this study to discretize the integral terms of Eq. (10), leading to the following discretized form:

$$\frac{dN_{kj}}{dt} = \sum_{j'=-\infty}^{\infty} \sum_{\substack{l \geq m \\ x_{k-1} \leq x_l + x_m \leq x_{k+1}}} \left(1 - \frac{1}{2} \delta_{l,m}\right) \eta_{l,m} F_{l,m,j-j',j'} N_{l,j-j'} N_{m,j'} - \sum_{j'=-\infty}^{\infty} \sum_{l=1}^M F_{k,l,j,j'} N_{k,j} N_{l,j'}, \quad (11)$$

where indices l and m refer to the size bins, δ is the Kronecker delta, $\eta_{l,m}$ is a property distribution factor between two size bins (Kumar and Ramkrishna, 1996), and M is the total number of the size bins. If coagulation is induced by thermal energy (i.e., Brownian coagulation), the collision frequency β^{Br} is given by (Fuchs, 1989):

$$\beta_{kl}^{\text{Br}} = 4\pi(r_k + r_l)(D_{p,k} + D_{p,l}) \left(\frac{r_k + r_l}{r_k + r_l + \sqrt{g_k^2 + g_l^2}} + \frac{4(D_{p,k} + D_{p,l})}{(r_k + r_l)\sqrt{\bar{v}_{p,k}^2 + \bar{v}_{p,l}^2}} \right)^{-1} \quad (12)$$

where D_p is the particle diffusion coefficient, g is the particle mean traveling distance, and \bar{v}_p is the particle thermal speed in air. Coagulation of charged particles is influenced by electrostatic particle-particle interactions. This effect can be accounted for by multiplying the collision frequency with the collision efficiency, α^{Br} (Fuchs, 1989; Seinfeld and Pandis, 2006):

$$\alpha_{kl}^{\text{Br}} = \frac{u}{e^u - 1} \quad (13)$$

$$\text{with } u = \frac{j_k j_l e^2}{4\pi\epsilon_0 \epsilon (r_k + r_l) k_B T}.$$

In Eq. (13), u indicates the relative importance between electrostatic potential energy and thermal energy in coagulation.

2.3.2 Monivariate population balance model

The time-evolution of the size distribution of particles can be estimated using a monivariate population balance model, with only the particle volume as the variable (Kumar and Ramkrishna, 1996):

$$\frac{dN_k}{dt} = \sum_{\substack{l \geq m \\ X_{k-l} \leq X_l + X_m \leq X_{k+l}}} \left(1 - \frac{1}{2} \delta_{l,m}\right) \eta_{l,m} F_{l,m} N_l N_m - \sum_{l=1}^M F_{k,l} N_k N_l. \quad (14)$$

The coagulation frequency can be simply corrected using the mean charge of particles. However, the collision efficiency computed with the mean charge can be different from that with the particle charge distributions (Matsoukas, 1997). To include effects of the particle charge distributions on the coagulation frequency, Eq. (13) can be replaced by the average collision efficiency $\bar{\alpha}$ (Clement et al., 1995), which involves interaction of all charged particles of size k with any charged particles of size l .

$$\bar{\alpha}_{kl}^{\text{Br}} = 1 + \frac{\sum_{j_k j_l \neq 0} N_{k,j_k} N_{l,j_l} (\alpha_{kl}^{\text{Br}} - 1)}{\sum_{j_k} N_{k,j_k} \sum_{j_l} N_{l,j_l}}. \quad (15)$$

The particle charge distributions needed to calculate $\bar{\alpha}^{\text{Br}}$ can be obtained by assuming a Gaussian distribution:

$$N_{kj} = \frac{\sum_j N_{k,j}}{\sqrt{2\pi}\sigma_k} \exp\left(-\frac{(j - J_k)^2}{2\sigma_k^2}\right) \quad (16)$$

with

$$\sigma^2 = y + \frac{1}{2\lambda}.$$

2.4 Approaches to couple particle charging with coagulation kinetics

Figure 1 shows three approaches which can be used to predict the time-evolution of the charge and size distributions of particles in the atmosphere. All the approaches can be used to simulate charging and coagulation kinetics of atmospheric particles carrying contaminants, including radioactive particles. Approach 1 is a rigorous scheme that simultaneously computes both charge accumulation and coagulation rates of particles using the ion balance model (Eqs. 1 and 2), the charge balance model (Eq. 5), and the bivariate population balance model (Eq. 11). Approach 2 is a simplified scheme of Approach 1, which can be used to predict the particle charge distribution using the mean charge of particles (Eq. 7) and the Gaussian distribution (Eq. 16). In order to easily simulate the coagulation of charged particles, Approach 2 employs the monovariate population balance model (Eq. 14) that corrects the collision frequency using the average collision efficiency (Eq. 15). Approach 2 can be simplified to Approach 3 by assuming that charge accumulation rates of particles instantaneously reach a steady state, with a timescale based on 5 times larger than τ from Eq. (8). The steady-state particle charge distribution can be approximated by Eqs. (9) and (16). In Approach 3, the collision frequency is multiplied by the average collision efficiency to include the influence of electrostatic forces on coagulation.

3 Results and discussion

3.1 Methods to simulate particle charging

The three approaches attained above employ different methods to simulate charging of particles. These methods (Eq. (5) in Approach 1, Eqs. (7) and (16) in Approach 2, and Eqs. (9) and (16) in Approach 3) were evaluated by comparing their prediction results with measurements obtained using radioactive charge neutralizers (Liu and Pui, 1974; Wiedensohler and Fissan, 1991; Alonso et al., 1997) and radioactive particles

Charging and coagulation of radioactive and nonradioactive particles

Y.-H. Kim et al.

Title Page

Abstract

Introduction

Conclusions

References

Tables

Figures

◀

▶

◀

▶

Back

Close

Full Screen / Esc

Printer-friendly Version

Interactive Discussion

(Gensdarmes et al., 2001). Initial conditions for the simulations were determined from the measurements. The properties of ions observed during the measurements are shown in Table 1. For the measurements providing the values of ion mass, $\beta_{k,j}^{\pm}$ was calculated using Fuchs (1963) and Hoppel and Frick (1986). However, the mass of ions was not measured during the experiments performed by Gensdarmes et al. (2001). In these experiments, $\beta_{k,j}^{\pm}$ was estimated using analytical equations given by Gunn (1954) and Harrison and Carslaw (2003).

3.1.1 Diffusion-charging mechanism

Figure 2 shows the steady-state charge distributions of nonradioactive particles over a wide size range. Here, the particles were charged by the diffusion charging mechanism. For particles larger than approximately 40 nm in diameter, the prediction results of all approaches were in good agreement with the measurements (Fig. 2a and b). Below 40 nm particle size, Approach 1 accurately forecasted the particle charge distributions, but Approaches 2 and 3 underestimated the number concentrations of the negatively charged particles (Fig. 2a) although the mean charge values of the particles given by all approaches were comparable. Similar discrepancies were observed for the number concentrations of the positively charged particles smaller than about 25 nm (not shown).

Analysis of the discrepancies suggests that they originate from the standard deviation involved in the Gaussian distribution (Eq. 16). At a given temperature, the width of the particle charge distributions can be significantly influenced by three parameters: the particle size, ion mass, and ion mobility (Wiedensohler and Fissan, 1991). In Approaches 2 and 3, however, the effects of the ion properties are not involved, so particle size primarily drives the standard deviation, which can differ from what Approach 1 gives. When Approaches 2 and 3 used the standard deviation values obtained by Approach 1, their simulation results became closer to the measurements, although the discrepancies are still seen for negatively and positively charged particles smaller than about 20 nm.

Charging and coagulation of radioactive and nonradioactive particles

Y.-H. Kim et al.

Title Page

Abstract

Introduction

Conclusions

References

Tables

Figures

◀

▶

◀

▶

Back

Close

Full Screen / Esc

Printer-friendly Version

Interactive Discussion



3.1.2 Competition of self-charging and diffusion-charging mechanisms

In our previous work (Kim et al., 2014, 2015), it has been shown that Approaches 1 and 3 can reliably simulate charging of radioactive particles. Thus, in this study, we focused on evaluating the validity of Approach 2 with the experiments of Gensdarmes et al. (2001) who measured the charge distributions of ^{137}Cs particles under various ionizing conditions. Ionizing rates of air molecules were estimated using a linear energy transfer equation for energetic electrons emitted by beta decay (Kim et al., 2015). Results of Approach 1 were included as a reference.

Figure 3 shows the charge accumulation on radioactive particles under two ionizing conditions: $q_1 = 3.7 \times 10^8 \text{ m}^{-3} \text{ s}^{-1}$ and $q_1 = 7.1 \times 10^6 \text{ m}^{-3} \text{ s}^{-1}$. Approach 2 predictions are in good agreement with observations and Approach 1 values. During the measurements, the self-charging rate of the radioactive particles was constant because of the long half-life of ^{137}Cs (approximately 30 years), suggesting that changes in their charge accumulation rates may be dominated by diffusion charging rates. The ion concentrations in air can rapidly increase at the high ionizing rate considered, suggesting that the diffusion charging rate of the ^{137}Cs particles quickly increased and then became comparable to their self-charging rate (Eq. 7). The charge accumulation on the radioactive particles promptly reached a steady-state value, and the particle charge distribution was similar to the initial condition (Fig. 4). In contrast, the time required to reach the steady-state value was much longer at the low ionizing rate considered; hence, the particle charge distribution shifted to the right in Fig. 4, i.e., more positive charge. The agreement observed in Fig. 4 between simulation results by Approach 2 and experimental data by Gensdarmes et al. (2001) suggests that Approach 2 can accurately forecast the competition between self- and diffusion charging on submicron particles carrying radionuclides, and precisely predict the particle charge distributions.

Charging and coagulation of radioactive and nonradioactive particles

Y.-H. Kim et al.

Title Page

Abstract

Introduction

Conclusions

References

Tables

Figures

◀

▶

◀

▶

Back

Close

Full Screen / Esc

Printer-friendly Version

Interactive Discussion

higher than that of the positively charged 3 nm particles. The concentrations of larger particles (e.g., charged and uncharged 6 nm particles) increased over time because of the size growth of small particles due to coagulation, as well as the diffusion-charging mechanism. These evolution patterns predicted by Approach 1 were in good agreement with the prediction results given by the analytical solution. As can be seen in Figs. 2 and 5, the ion balance and charge balance models of Approach 1 accurately predicted the diffusion charging of nanoparticles, suggesting that the numerical solution of the bivariate population balance model (Eq. 11) reliably predicts coagulation of particles acquiring charge.

3.2.2 Average collision efficiency of Approaches 2 and 3

Approaches 2 and 3 employ an average collision efficiency and are coupled to the monovariate, instead of the bivariate, population balance model. These approaches provided accurate particle charge distributions for various cases (e.g., Figs. 2 and 4; Kim et al., 2014), suggesting that their validity may be highly influenced by the accuracy of the average collision efficiency. Thus, we compared simulation results of Approach 2 with those of Approach 1 to check if the average collision efficiency (Eq. 15) can appropriately account for the influence of the charge distributions of particles on their size growth via coagulation. For comparison, simulation results of Approach 2 using the mean charge (Eq. 13), as well as those for uncharged particles, were included. Similarly to Oron and Seinfeld (1989a, b), we assumed monodispersed initial size distributions ($d_p = 0.1 \mu\text{m}, 0.5, 1 \mu\text{m}, N_t = 10^7 \text{cm}^{-3}$, and $n_0 = 10^{10} \text{cm}^{-3}$). The geometrical grids ($x_{k+1} = 2x_k$) were used to cover a wide particle-size range. Other basic assumptions were similar to those considered for the validation test of Approach 1.

Figure 8 shows the time-evolution of the particle size distributions induced by particle charging and coagulation. The simulation conditions led to the accumulation of more negative than positive charges on the particles. At $t = 1 \text{ min}$, the number fraction of the negatively charged particles was 0.7, while that of the positively charged and uncharged particles was 0.16 and 0.14, respectively. Thus, the size growth of the particles

Charging and coagulation of radioactive and nonradioactive particles

Y.-H. Kim et al.

Title Page

Abstract

Introduction

Conclusions

References

Tables

Figures

◀

▶

◀

▶

Back

Close

Full Screen / Esc

Printer-friendly Version

Interactive Discussion



Charging and coagulation of radioactive and nonradioactive particles

Y.-H. Kim et al.

Title Page

Abstract

Introduction

Conclusions

References

Tables

Figures

◀

▶

◀

▶

Back

Close

Full Screen / Esc

Printer-friendly Version

Interactive Discussion



predictions by Approaches 2 and 3 were different from the measurements. The particle size distributions predicted by all the approaches were similar (not shown). It can be concluded that the Gaussian distribution used in Approaches 2 and 3 cannot accurately predict the charge distributions of very small particles (see Fig. 2). Thus, Approaches 2 and 3 should not be used for particles smaller than 40 nm.

As shown in Figs. 2–5, Approach 1 can accurately predict the charge accumulation rate of radioactive and nonradioactive particles in the free-molecule, transition, and continuum regimes. Approach 1 employs the interpolation formula of Fuchs that can be used to compute the collision frequency of the particles in these regimes, revealing that this approach can also precisely predict the charge distribution of larger particles undergoing coagulation. These results suggest that Approach 1 can be a reasonable option to simultaneously simulate charging and coagulation of particles of any size in laboratory-scale experiments.

3.3.2 Charging and coagulation of nonradioactive particles in urban atmosphere

Hoppel (1985) simulated charging of 0.06 μm urban aerosols by diffusion charging; however, effects of coagulation on their steady-state charge distribution were excluded from the simulation. Changes in the particle charge and size distributions by charging and coagulation were investigated in this work on the basis of the simulation of Hoppel (1985) for comparison. The simulation time was approximately 100 min, but for completeness, we repeated and extended the Hoppel (1985) simulation to 1 day. The extended results were compared with prediction results of Approach 1, which involves the effects of coagulation on the particle charge distribution. It was assumed that cosmic rays and natural radioactivity generate ion pairs in the atmosphere, giving $q_b \approx 10^7 \text{ m}^{-3} \text{ s}^{-1}$ (Hoppel, 1985).

Figure 11 presents changes in the particle charge and size distributions vs. time. The simulation results performed by Hoppel (1985) showed that the particle charge distribution approached its steady-state value after approximately 90 min. However, as

ticle charge distribution was slightly moved to the left. Because the decay rates of the highly radioactive particles were reduced over time, their self-charging rates also decreased, and this led to the slight movement of the charge distribution to the left in Fig. 13a.

5 The discrepancies between the predictions of Approach 1 and Greenfield (1956) result mainly from the ion-particle attachment coefficient used in the simulation. The values assumed by Greenfield (1956) were beyond the ion-particle attachment coefficient found by other researchers (e.g., Hoppel and Frick, 1986), leading to the discrepancies observed (Kim et al., 2015).

10 Beta radiation caused by radioactive decay rapidly increased the ion concentrations, thereby enhancing the electrical conductivity in the atmosphere (Fig. 14). In contrast to the case shown in Fig. 12, the ion concentrations and air conductivity significantly decreased with time because the ionization rate of air molecules decreased considerably, and ion-ion recombination was responsible for the change in the concentrations. Nevertheless, the air conductivity enhancement by beta radiation was much higher than that by cosmic rays and natural radioactivity.

15 After the Chernobyl and Fukushima accidents, short- and long-range transport of particles carrying radionuclides, such as ^{137}Cs and ^{134}Cs , affected the electrical properties of the local atmosphere in many places (Israelsson and Knudsen, 1986; Yamauchi et al., 2012). In particular, beta radiation led to significant changes in the electrical conductivity and potential gradient in the local atmosphere (Kim et al., 2015). Israelsson et al. (1987) suggested that an increase in the electrical conductivity led to enhancement of lightning activities at radioactively contaminated sites in Sweden. These observations reveal that the approaches developed in this study can be employed to investigate the influence of radionuclides on electrification phenomena in the atmosphere.

Charging and coagulation of radioactive and nonradioactive particles

Y.-H. Kim et al.

Title Page

Abstract	Introduction
Conclusions	References
Tables	Figures

◀ ◻ ▶

◀ ◻ ▶

Back	Close
------	-------

Full Screen / Esc

Printer-friendly Version

Interactive Discussion



Steady-state assumption of radioactive particle charging

The steady-state assumption of particle charging can be useful to simulate coagulation of radioactive particles in model studies of radioactivity transport. Charging and coagulation kinetics of radioactive particles were investigated using Approaches 2 and 3 to evaluate the validity of the steady-state assumption of radioactive particle charging. For comparison, the size growth of particles by coagulation was simulated by assuming the Boltzmann charge distribution.

We used the simulation condition employed to validate the average collision efficiency, but additionally presumed that radioactive decay of ^{134}Cs is responsible for the ionization of air molecules. The specific radioactivity of ^{134}Cs was obtained from Clement and Harrison (1992). The ionization rate of ^{134}Cs was estimated according to Kim et al. (2015). Under these conditions, Eq. (8) revealed that $5\tau \approx 4.3$ ms. Thus, we assumed that charge accumulation rates of ^{134}Cs particles instantaneously reach steady state, and evaluated this assumption for the simulation conditions of $X \approx 0.7$ and ion concentration given by $q_l = I_{\text{Cs-134}} \times \eta_{\text{Cs-134}} \times N_t$ (a function of ion-particle attachment, ion-ion recombination, and beta radiation).

Figure 15 shows the charge and size distributions of the ^{134}Cs particles after 2 h of evolution. The prediction results of Approach 3 were different from those of the case assuming the Boltzmann charge distribution, but agreed well with those of Approach 2, suggesting that the steady-state assumption of radioactive particle charging can be valid if τ is small. We also tested the assumption of Approach 3 using different initial conditions (e.g., $d_p = 0.3 \mu\text{m}$), and the agreement was still maintained (not shown).

3.4 Computational costs

The computational costs to predict transport of particles containing contaminants depends on the number of ordinary differential equations (ODEs) solved during simulation. Thus, the number of ODEs involved in the three approaches was evaluated by assuming 30 size bins, which corresponds to those used in the two-moment aerosol

Charging and coagulation of radioactive and nonradioactive particles

Y.-H. Kim et al.

Title Page

Abstract

Introduction

Conclusions

References

Tables

Figures

◀

▶

◀

▶

Back

Close

Full Screen / Esc

Printer-friendly Version

Interactive Discussion



Charging and coagulation of radioactive and nonradioactive particles

Y.-H. Kim et al.

Title Page

Abstract

Introduction

Conclusions

References

Tables

Figures

◀

▶

◀

▶

Back

Close

Full Screen / Esc

Printer-friendly Version

Interactive Discussion



processes can change their important physical and electrical properties, such as size and charge. This study has shown three approaches with a wide range of complexity and applications to involve the mutual effects of charging and coagulation processes in the simulation of particle charge and size distributions vs. time. Depending on the initial conditions, these approaches can be employed to accurately predict the behavior of atmospheric particles carrying radioactive contaminants. We have shown the approaches to be applicable to a wide variety of atmospheric (laboratory and field) applications. The accuracy of the approaches depends on the assumptions made to reduce computational cost. The developed approaches can be readily incorporated into microphysical and transport models of any scale to account for charging phenomena of atmospheric particles.

Acknowledgements. This work was supported by the Defense Threat Reduction Agency under grant number DTRA1-08-10-BRCWMD-BAA. The manuscript has been co-authored by UT-Battelle, LLC, under Contract No. DEAC05-00OR22725 with the US Department of Energy.

References

- Alonso, M.: Simultaneous charging and Brownian coagulation of nanometre aerosol particles, *J. Phys. A-Math. Gen.*, 32, 1313–1327, doi:10.1088/0305-4470/32/8/003, 1999.
- Alonso, M., Kousaka, Y., Nomura, T., Hashimoto, N., and Hashimoto, T.: Bipolar charging and neutralization of nanometer-sized aerosol particles, *J. Aerosol Sci.*, 28, 1479–1490, doi:10.1016/S0021-8502(97)00036-0, 1997.
- Alonso, M., Hashimoto, T., Kousaka, Y., Higuchi, M., and Nomura, T.: Transient bipolar charging of a coagulating nanometer aerosol, *J. Aerosol Sci.*, 29, 263–270, doi:10.1016/S0021-8502(97)10007-6, 1998.
- Chin, C.-J., Yiacomini, S., and Tsouris, C: Shear-induced flocculation of colloidal particles in stirred tanks, *J. Colloid Interf. Sci.*, 206, 532–545, doi:10.1006/jcis.1998.5737, 1998.
- Clement, C. F. and Harrison, R. G.: The charging of radioactive aerosols, *J. Aerosol Sci.*, 23, 481–504, doi:10.1016/0021-8502(92)90019-R, 1992.

Charging and coagulation of radioactive and nonradioactive particles

Y.-H. Kim et al.

Title Page

Abstract

Introduction

Conclusions

References

Tables

Figures

◀

▶

◀

▶

Back

Close

Full Screen / Esc

Printer-friendly Version

Interactive Discussion



Clement, C. F., Clement, R. A., and Harrison, R.G.: Charge distributions and coagulation of radioactive aerosols, *J. Aerosol Sci.*, 26, 1207–1225, doi:10.1016/0021-8502(95)00525-0, 1995.

Fuchs, N. A.: On the stationary charge distribution on aerosol particles in a bipolar ionic atmosphere, *Geofis. Pura. Appl.*, 56, 185–193, doi:10.1007/BF01993343, 1963.

Fuchs, N. A.: *The Mechanics of Aerosols*, Dover Publications, 1989.

Gensdarmes, F., Boulaud, D., and Renoux, A.: Electrical charging of radioactive aerosols—comparison of the Clement–Harrison models with new experiments, *J. Aerosol Sci.*, 32, 1437–1458, doi:10.1016/S0021-8502(01)00065-9, 2001.

Greenfield, S. M.: Ionization of radioactive particles in the free air, *J. Geophys. Res.*, 61, 27–33, doi:10.1029/JZ061i001p00027, 1956.

Gunn, R.: Diffusion charging of atmospheric droplets by ions, and the resulting combination coefficients, *J. Meteorol.*, 11, 339–347, doi:10.1175/1520-0469(1954)011<0339:DCOADB>2.0.CO;2, 1954.

Harrison, R. G. and Carslaw, K. S.: Ion-aerosol-cloud processes in the lower atmosphere, *Rev. Geophys.*, 41, 1012, doi:10.1029/2002RG000114, 2003.

Hoppel, W. A.: Ion-aerosol attachment coefficients, ion depletion, and the charge distribution on aerosols, *J. Geophys. Res.*, 90, 5917–5923, doi:10.1029/JD090iD04p05917, 1985.

Hoppel, W. A. and Frick, G. M.: Ion-aerosol attachment coefficients and the steady-state charge distribution on aerosols in a bipolar ion environment, *Aerosol Sci. Tech.*, 5, 1–21, doi:10.1080/02786828608959073, 1986.

Israelsson, S. and Knudsen, E.: Effects of radioactive fallout from a nuclear power plant accident on electrical parameters, *J. Geophys. Res.*, 91, 11909–11910, doi:10.1029/JD091iD11p11909, 1986.

Israelsson, S., Schütte, T., Pislser, E., and Lundquist, S.: Increased occurrence of lightning flashes in Sweden during 1986, *J. Geophys. Res.*, 92, 10996–10998, doi:10.1029/JD092iD09p10996, 1987.

Kim, Y.-H., Yiacoumi, S., Lee, I., McFarlane, J., and Tsouris, C.: Influence of radioactivity on surface charging and aggregation kinetics of particles in the atmosphere, *Environ. Sci. Technol.*, 48, 182–189, doi:10.1021/es4047439, 2014.

Kim, Y.-H., Yiacoumi, S., and Tsouris, C.: Surface charge accumulation of particles containing radionuclides in open air, *J. Environ. Radioactiv.*, 143, 91–99, doi:10.1016/j.jenvrad.2015.02.017, 2015.

**Charging and
coagulation of
radioactive and
nonradioactive
particles**

Y.-H. Kim et al.

Title Page

Abstract

Introduction

Conclusions

References

Tables

Figures

◀

▶

◀

▶

Back

Close

Full Screen / Esc

Printer-friendly Version

Interactive Discussion



Kumar, S. and Ramkrishna, D.: On the solution of population balance equations by discretization – I, a fixed pivot technique, *Chem. Eng. Sci.*, 51, 1311–1332, doi:10.1016/0009-2509(96)88489-2, 1996.

Kweon, H., Yiacomini, S., Lee, I., McFarlane, J., and Tsouris, C.: Influence of surface potential on the adhesive force of radioactive gold surfaces, *Langmuir*, 29, 11876–11883, doi:10.1021/la4008476, 2013.

Laakso, L., Mäkelä, J. M., Pirjola, L., and Kulmala, M.: Model studies on ion-induced nucleation in the atmosphere, *J. Geophys. Res.*, 107, 4427, doi:10.1029/2002JD002140, 2002.

Liu, B. Y. and Pui, D. Y.: Equilibrium bipolar charge distribution of aerosols, *J. Colloid Interf. Sci.*, 49, 305–312, doi:10.1016/0021-9797(74)90366-X, 1974.

Matsoukas, T.: The coagulation rate of charged aerosols in ionized gases, *J. Colloid Interf. Sci.*, 187, 474–483, doi:10.1006/jcis.1996.4723, 1997.

Ooe, H., Seki, R., and Ikeda, N.: Particle-size distribution of fission products in airborne dust collected at Tsukuba from April to June 1986, *J. Environ. Radioactiv.*, 6, 219–223, doi:10.1016/0265-931X(88)90078-1, 1988.

Oron, A. and Seinfeld, J. H.: The dynamic behavior of charged aerosols: II, numerical solution by the sectional method, *J. Colloid Interf. Sci.*, 133, 66–79, doi:10.1016/0021-9797(89)90282-8, 1989a.

Oron, A. and Seinfeld, J. H.: The dynamic behavior of charged aerosols: III, simultaneous charging and coagulation, *J. Colloid Interf. Sci.*, 133, 80–90, doi:10.1016/0021-9797(89)90283-X, 1989b.

Pruppacher, H. R. and Klett, J. D.: *Microphysics of Clouds and Precipitation*, Kluwer Acad., Norwell, Mass., 1997.

Renard, J.-B., Tripathi, S. N., Michael, M., Rawal, A., Berthet, G., Fullekrug, M., Harrison, R. G., Robert, C., Tagger, M., and Gaubicher, B.: In situ detection of electrified aerosols in the upper troposphere and stratosphere, *Atmos. Chem. Phys.*, 13, 11187–11194, doi:10.5194/acp-13-11187-2013, 2013.

Seinfeld, J. H. and Pandis, S. N.: *Atmospheric Chemistry and Physics: From Air Pollution to Climate Change*, John Wiley and Sons, New Jersey, 2006.

Taboada-Serrano, P., Chin, C., Yiacomini, S., and Tsouris, C.: Modeling aggregation of colloidal particles, *Curr. Opin. Colloid In.*, 10, 123–132, doi:10.1016/j.cocis.2005.07.003, 2005.

Charging and coagulation of radioactive and nonradioactive particles

Y.-H. Kim et al.

Title Page

Abstract

Introduction

Conclusions

References

Tables

Figures

◀

▶

◀

▶

Back

Close

Full Screen / Esc

Printer-friendly Version

Interactive Discussion



Tsouris, C., Yiacoymi, S., and Scott, T.: Kinetics of heterogeneous magnetic flocculation using a bivariate population-balance equation, *Chem. Eng. Commun.*, 137, 147–159, doi:10.1080/00986449508936373, 1995.

Vanni, M.: Approximate population balance equations for aggregation–breakage processes, *J. Colloid Interf. Sci.*, 221, 143–160, doi:10.1006/jcis.1999.6571, 2000.

Vasilakos, P., Kim, Y.-H., Pierce, J., Yiacoymi, S., Tsouris, C., and Nenes, A.: The impact of radioactive charging on the microphysical evolution and transport of radioactive aerosols, in preparation, 2015.

Walker, M. E., McFarlane, J., Glasgow, D. C., Chung, E., Taboada-Serrano, P., Yiacoymi, S., and Tsouris, C.: Influence of radioactivity on surface interaction forces, *J. Colloid Interf. Sci.*, 350, 595–598, doi:10.1016/j.jcis.2010.06.042, 2010.

Wiedensohler, A. and Fissan, H. J.: Bipolar charge distributions of aerosol particles in high-purity argon and nitrogen, *Aerosol Sci. Tech.*, 14, 358–364, doi:10.1080/02786829108959498, 1991.

Yair, Y. and Levin, Z.: Charging of polydispersed aerosol particles by attachment of atmospheric ions, *J. Geophys. Res.*, 94, 13085–13091, doi:10.1029/JD094iD11p13085, 1989.

Yamauchi, M., Takeda, M., Makino, M., Owada, T., and Miyagi, I.: Settlement process of radioactive dust to the ground inferred from the atmospheric electric field measurement, *Ann. Geophys.*, 30, 49–56, doi:10.5194/angeo-30-49-2012, 2012.

Yeh, H. C., Newton, G. J., Raabe, O. G., and Boor, D. R.: Self-charging of ^{198}Au -labeled monodisperse gold aerosols studied with a miniature electrical mobility spectrometer, *J. Aerosol Sci.*, 7, 245–253, doi:10.1016/0021-8502(76)90039-2, 1976.

Yoshenko, V. I., Kashparov, V. A., Protsak, V. P., Lundin, S. M., Levchuk, S. E., Kadygrib, A. M., Zvarich, S. I., Khomutinin, X. V., Maloshtan, I. M., Lanshin, V. P., Kovtun, M. V., and Tschiersch, J.: Resuspension and redistribution of radionucleotides during grassland and forest fires in the Chernobyl exclusion zone, Part I: Fire experiments, *J. Environ. Radioactiv.*, 86, 143–163, doi:10.1016/j.jenvrad.2005.08.003, 2006a.

Yoshenko, V. I., Kashparov, V. A., Levchuk, S. E., Glukhovskiy, A.S., Khomutni, Y. V., Protsak, V. P., Lundin, S. M., and Tschiersch, J.: Resuspension and redistribution of radionucleotides during grassland and forest fires in the Chernobyl exclusion zone, Part II: Modeling the transport process, *J. Environ. Radioactiv.*, 87, 260–278, doi:10.1016/j.jenvrad.2005.12.003, 2006b.

**Charging and
coagulation of
radioactive and
nonradioactive
particles**

Y.-H. Kim et al.

Title Page

Abstract

Introduction

Conclusions

References

Tables

Figures



Back

Close

Full Screen / Esc

Printer-friendly Version

Interactive Discussion

Charging and coagulation of radioactive and nonradioactive particles

Y.-H. Kim et al.

Title Page

Abstract

Introduction

Conclusions

References

Tables

Figures

◀

▶

◀

▶

Back

Close

Full Screen / Esc

Printer-friendly Version

Interactive Discussion



Table 1. Properties of ions used for experimental observations.

References	Positive ions		Negative ions	
	Mass (AMU)	Mobility ($\text{cm}^2 \text{V}^{-1} \text{s}^{-1}$)	Mass (AMU)	Mobility ($\text{cm}^2 \text{V}^{-1} \text{s}^{-1}$)
Alonso et al. (1997)	150	1.15	80	1.65
Liu and Pui (1974) ^a	140	1.4	101	1.6
Wiedensohler and Fissan (1991)	140	1.4	101	1.6
Gensdarmes et al. (2001)	–	1.19	–	1.54

^a The properties of ions were obtained from Wiedensohler and Fissan (1991), who used a radioactive neutralizer similar to that employed by Liu and Pui (1974).

Charging and coagulation of radioactive and nonradioactive particles

Y.-H. Kim et al.

Title Page

Abstract

Introduction

Conclusions

References

Tables

Figures

◀

▶

◀

▶

Back

Close

Full Screen / Esc

Printer-friendly Version

Interactive Discussion

Table 3. Computational costs of the approaches used.

Example: 30 size bins		Approach 1	Approach 2	Approach 3
The number of ODEs	Ion balance model	2	2	–
	Charge balance model	$30 \times 31 = 930$	30	–
	Population balance model		30	30
	Total	932	62	30
Computational time for urban aerosol ^{a, b} (s)		12 724.2	302.6	8.5

^a Simulation conditions: $d_g = 0.116 \mu\text{m}$, $\sigma_g = 1.46$, $N_t = 6.718 \times 10^9 \text{ m}^{-3}$ and $q = 10^7 \text{ m}^{-3} \text{ s}^{-1}$ (Kim et al., 2015). The simulation time is 6 h.

^b Computational resources: Intel(R) Core(TM)2 Duo CPU E6850 @ 3.00 GHz with 4GB RAM and Matlab ODE solver.

Charging and coagulation of radioactive and nonradioactive particles

Y.-H. Kim et al.

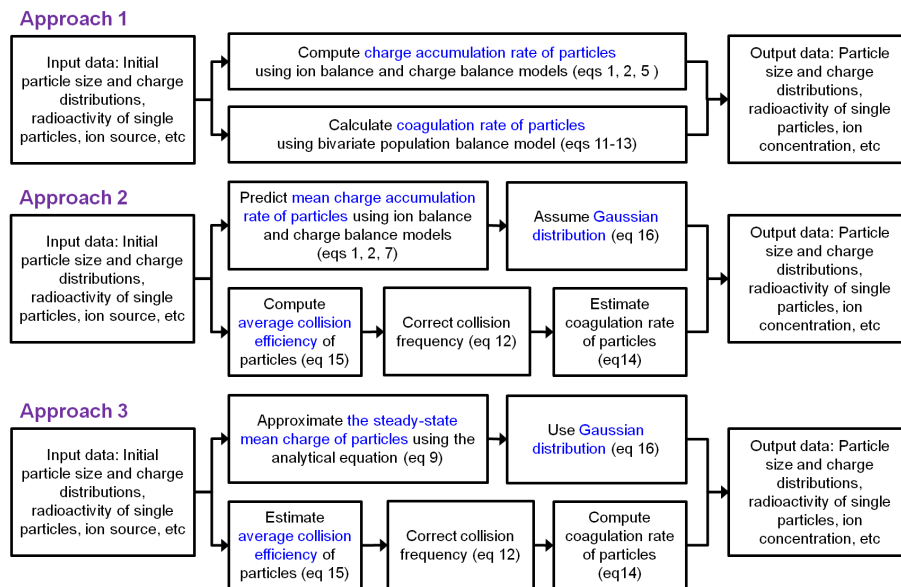


Figure 1. Three approaches to predict time-dependent changes in the particle size and charge distributions in the atmosphere.

Title Page	
Abstract	Introduction
Conclusions	References
Tables	Figures
◀	▶
◀	▶
Back	Close
Full Screen / Esc	
Printer-friendly Version	
Interactive Discussion	



Charging and coagulation of radioactive and nonradioactive particles

Y.-H. Kim et al.

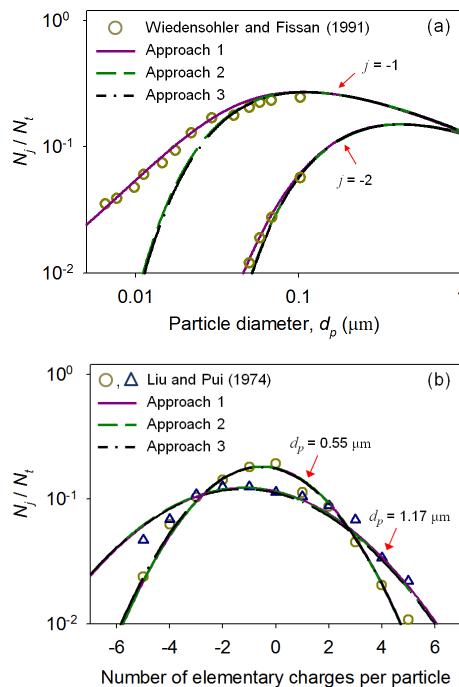


Figure 2. Steady-state charge distributions of particles capturing positive and negative ions. The symbols represent the measurements of the charge distributions of particles.

Charging and coagulation of radioactive and nonradioactive particles

Y.-H. Kim et al.

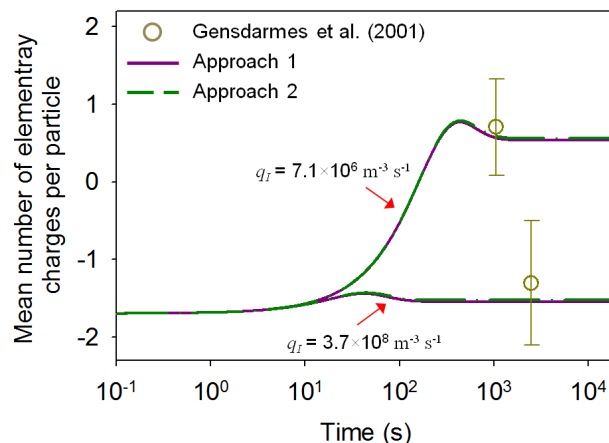


Figure 3. Charge accumulation on ^{137}Cs particles under two ionizing conditions: $q_I = 7.1 \times 10^6 \text{ m}^{-3} \text{ s}^{-1}$ and $q_I = 3.7 \times 10^8 \text{ m}^{-3} \text{ s}^{-1}$ ($d_p = 0.82 \mu\text{m}$; $\eta_{\text{Cs-137}} = 12.8 \text{ mBq}$). The symbols represent the mean value of the particle charge distributions measured by Gensdarmes et al. (2001).

Title Page

Abstract

Introduction

Conclusions

References

Tables

Figures

◀

▶

◀

▶

Back

Close

Full Screen / Esc

Printer-friendly Version

Interactive Discussion

Charging and coagulation of radioactive and nonradioactive particles

Y.-H. Kim et al.

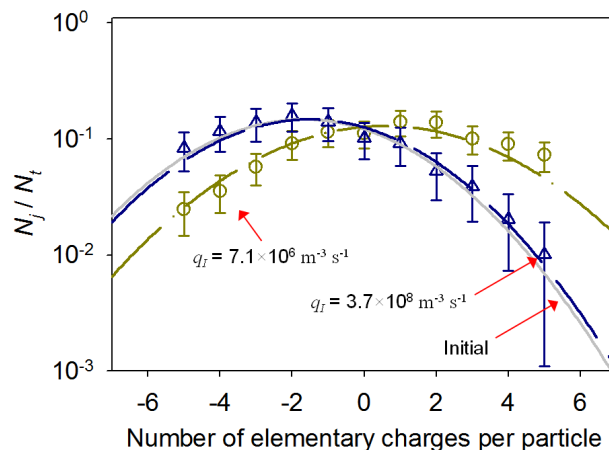


Figure 4. Charge distributions of ^{137}Cs particles under two ionizing conditions: $q_I = 7.1 \times 10^6 \text{ m}^{-3} \text{ s}^{-1}$ and $q_I = 3.7 \times 10^8 \text{ m}^{-3} \text{ s}^{-1}$ ($d_p = 0.82 \mu\text{m}$; $\eta_{\text{Cs-137}} = 12.8 \text{ mBq}$). The prediction results of Approach 2 were compared with the measurements of Gensdarmes et al. (2001).

Title Page

Abstract

Introduction

Conclusions

References

Tables

Figures

◀

▶

◀

▶

Back

Close

Full Screen / Esc

Printer-friendly Version

Interactive Discussion

Charging and coagulation of radioactive and nonradioactive particles

Y.-H. Kim et al.

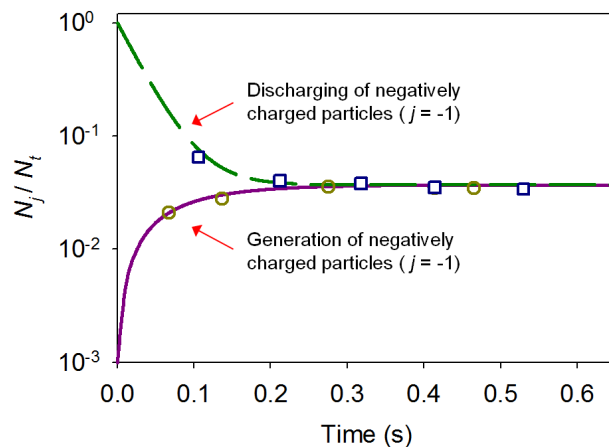


Figure 5. Timescale to reach steady-state charge accumulation rates of 7.1 nm nanoparticles. The lines are the simulation results of Approach 1. The symbols are the measurements of Alonso et al. (1997). Charging timescales were estimated using Eq. (8) ($\tau_{\text{charging}} = 0.042$ s and $\tau_{\text{discharging}} = 0.017$ s), as well as Approach 1 and the measurements.

Title Page

Abstract

Introduction

Conclusions

References

Tables

Figures

◀

▶

◀

▶

Back

Close

Full Screen / Esc

Printer-friendly Version

Interactive Discussion

Charging and coagulation of radioactive and nonradioactive particles

Y.-H. Kim et al.

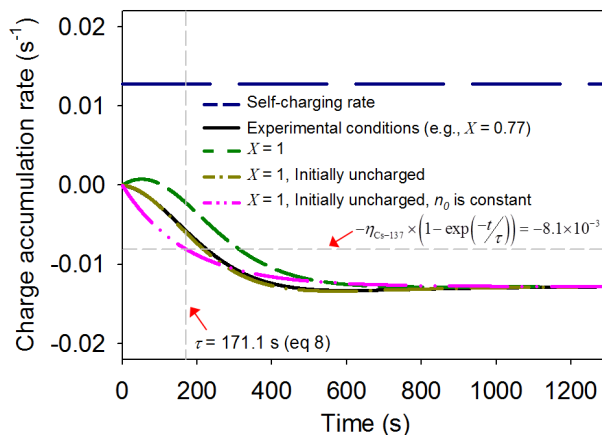


Figure 6. Charge accumulation rate of ^{137}Cs particles for each charging mechanism ($d_p = 0.82 \mu\text{m}$; $\eta_{\text{Cs-137}} = 12.8 \text{ mBq}$; $q_l = 7.1 \times 10^6 \text{ m}^{-3} \text{ s}^{-1}$). The assumptions used in Eq. (8) were applied to evaluate the validity of the equation. $\eta_{\text{Cs-137}}$ corresponds to the self-charging rate of the radioactive particles.

Title Page

Abstract

Introduction

Conclusions

References

Tables

Figures

◀

▶

◀

▶

Back

Close

Full Screen / Esc

Printer-friendly Version

Interactive Discussion



Charging and coagulation of radioactive and nonradioactive particles

Y.-H. Kim et al.

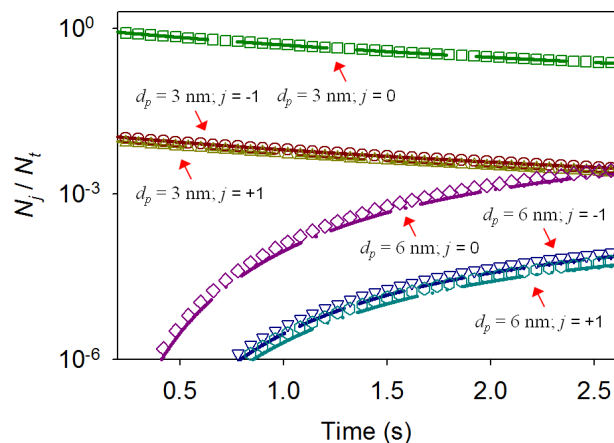


Figure 7. Validation of the numerical solution for the bivariate population balance model under a monodispersed initial condition ($d_p = 3$ nm, $N_t = 10^9$ cm $^{-3}$, and $n_0 = 10^{12}$ cm $^{-3}$). The lines and symbols represent the results of the analytical solution of Alonso (1999) and Eq. (11), respectively.

[Title Page](#)
[Abstract](#)
[Introduction](#)
[Conclusions](#)
[References](#)
[Tables](#)
[Figures](#)
[◀](#)
[▶](#)
[◀](#)
[▶](#)
[Back](#)
[Close](#)
[Full Screen / Esc](#)
[Printer-friendly Version](#)
[Interactive Discussion](#)

Charging and coagulation of radioactive and nonradioactive particles

Y.-H. Kim et al.

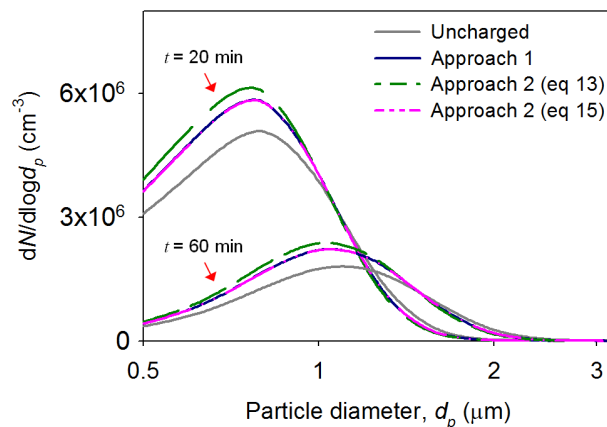


Figure 8. Time-evolution of the particle size distributions predicted by the monovariate population balance model with the average collision efficiency (Eq. 15) under a monodispersed initial condition ($d_p = 0.5 \mu\text{m}$, $N_t = 10^7 \text{cm}^{-3}$; $n_0 = 10^{10} \text{cm}^{-3}$). Approach 1 was used as a reference that includes the mutual effect of surface charging and coagulation on the particle size and charge distributions.

Title Page

Abstract

Introduction

Conclusions

References

Tables

Figures

◀

▶

◀

▶

Back

Close

Full Screen / Esc

Printer-friendly Version

Interactive Discussion

Charging and coagulation of radioactive and nonradioactive particles

Y.-H. Kim et al.

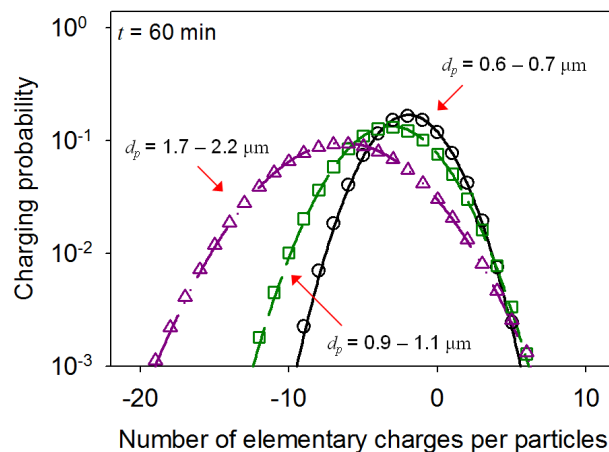


Figure 9. Charge distributions of particles undergoing coagulation under a monodispersed initial condition ($d_p = 0.5 \mu\text{m}$, $N_t = 10^7 \text{cm}^{-3}$; $n_0 = 10^{10} \text{cm}^{-3}$). The charging probability was obtained according to Renard et al. (2013). The lines and symbols represent the simulation results of Approaches 1 and 2, respectively. Three size bins are chosen to compare the simulation results of the approaches.

[Title Page](#)
[Abstract](#)
[Introduction](#)
[Conclusions](#)
[References](#)
[Tables](#)
[Figures](#)
[◀](#)
[▶](#)
[◀](#)
[▶](#)
[Back](#)
[Close](#)
[Full Screen / Esc](#)
[Printer-friendly Version](#)
[Interactive Discussion](#)

Charging and coagulation of radioactive and nonradioactive particles

Y.-H. Kim et al.

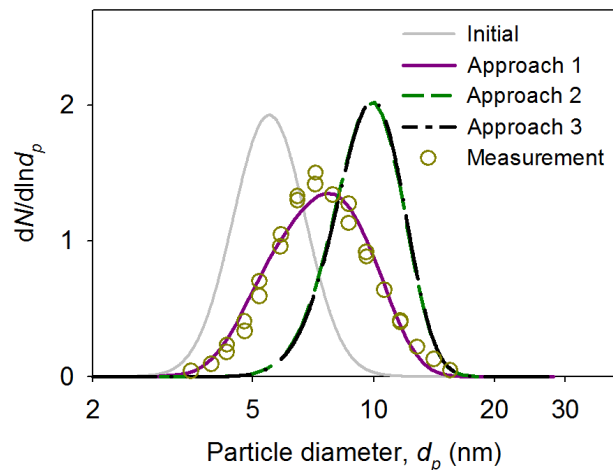


Figure 10. Evolution of the size distribution of negatively charged particles in a ^{241}Am radioactive neutralizer. For the initial condition, $d_g = 5.5$ nm, $\sigma_g = 1.23$, and $N_t = 5 \times 10^9$ cm $^{-3}$. The lines represent the simulation result of Approach 1. The symbols are the measurements of Alonso et al. (1998).

Title Page

Abstract

Introduction

Conclusions

References

Tables

Figures

◀

▶

◀

▶

Back

Close

Full Screen / Esc

Printer-friendly Version

Interactive Discussion

Charging and coagulation of radioactive and nonradioactive particles

Y.-H. Kim et al.

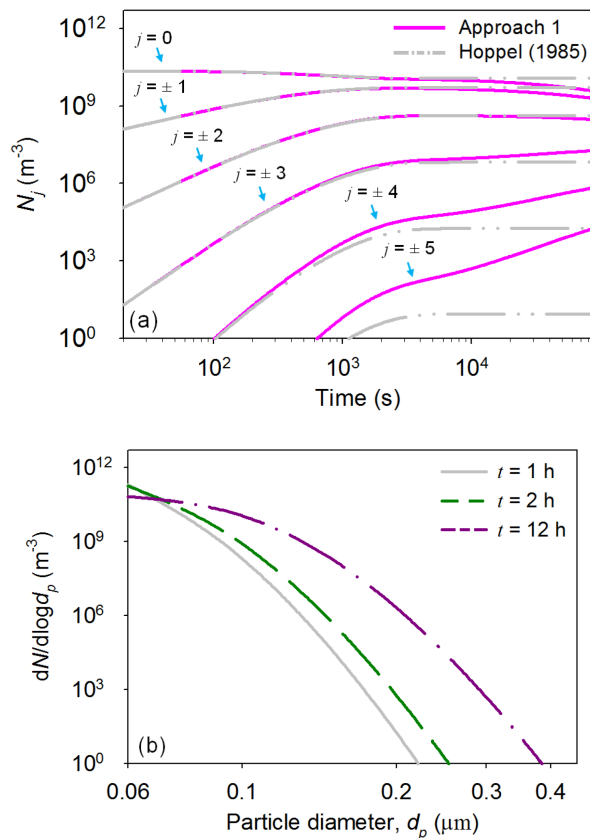


Figure 11. Time-evolution of the charge (a) and size (b) distributions of atmospheric particles in the postulated atmosphere of Hoppel (1985) ($d_p = 0.06 \mu\text{m}$, $N_t = 2.3 \times 10^{10} \text{m}^{-3}$; $q = 10^7 \text{m}^{-3} \text{s}^{-1}$). Approach 1 was used to involve the effects of coagulation on the Hoppel (1985) simulation.

Charging and coagulation of radioactive and nonradioactive particles

Y.-H. Kim et al.

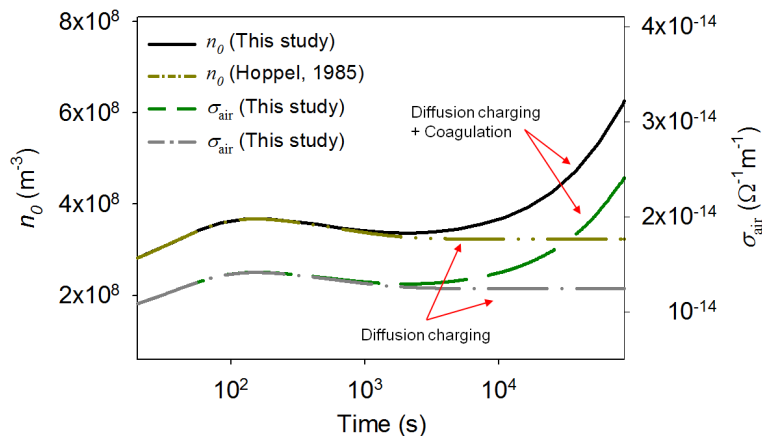


Figure 12. Time-evolution of the mean ion concentration, n_0 and air conductivity, σ_{air} in the postulated atmosphere of Hoppel (1985) ($d_p = 0.06 \mu\text{m}$, $N_t = 2.3 \times 10^{10} \text{m}^{-3}$; $q = 10^7 \text{m}^{-3} \text{s}^{-1}$).

Title Page

Abstract

Introduction

Conclusions

References

Tables

Figures

◀

▶

◀

▶

Back

Close

Full Screen / Esc

Printer-friendly Version

Interactive Discussion

Charging and coagulation of radioactive and nonradioactive particles

Y.-H. Kim et al.

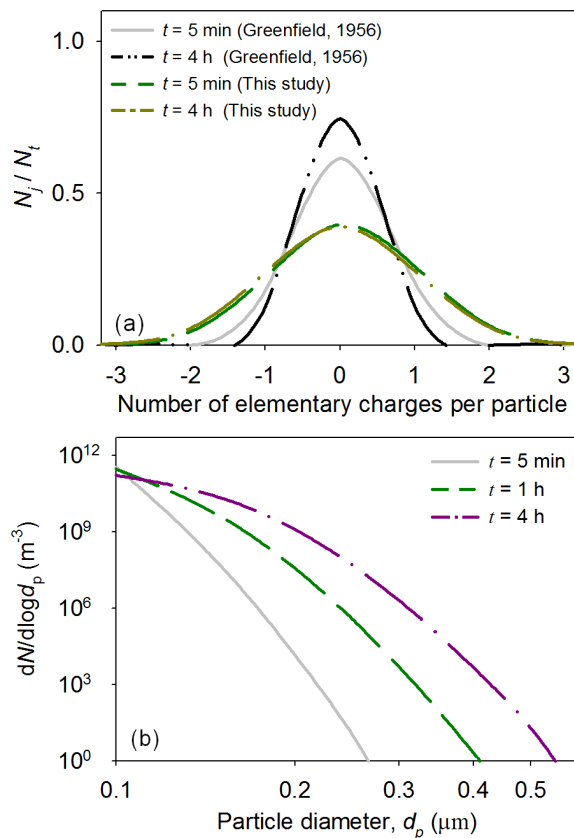


Figure 13. Time-evolution of the charge (a) and size (b) distributions of monodispersed radioactive particles at 6 km altitude ($d_p = 0.1 \mu m$, $N_t = 3.55 \times 10^{10} m^{-3}$; $I = 1.5 \times 10^4 s^{-1}$). Approach 1 was used to simultaneously simulate surface charging and coagulation of radioactive particles.

Charging and coagulation of radioactive and nonradioactive particles

Y.-H. Kim et al.

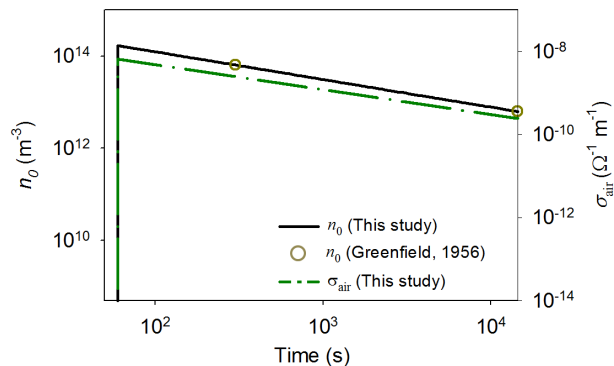


Figure 14. Time-evolution of the mean ion concentration, n_0 and air conductivity, σ_{air} induced by monodispersed radioactive particles at 6 km altitude ($d_p = 0.1 \mu\text{m}$, $N_t = 3.55 \times 10^{10} \text{m}^{-3}$; $I = 1.5 \times 10^4 \text{s}^{-1}$). The lines represent the simulation results of Approach 1. The symbols represent the estimation of Greenfield (1956).

[Title Page](#)
[Abstract](#)
[Introduction](#)
[Conclusions](#)
[References](#)
[Tables](#)
[Figures](#)
[◀](#)
[▶](#)
[◀](#)
[▶](#)
[Back](#)
[Close](#)
[Full Screen / Esc](#)
[Printer-friendly Version](#)
[Interactive Discussion](#)

Charging and coagulation of radioactive and nonradioactive particles

Y.-H. Kim et al.

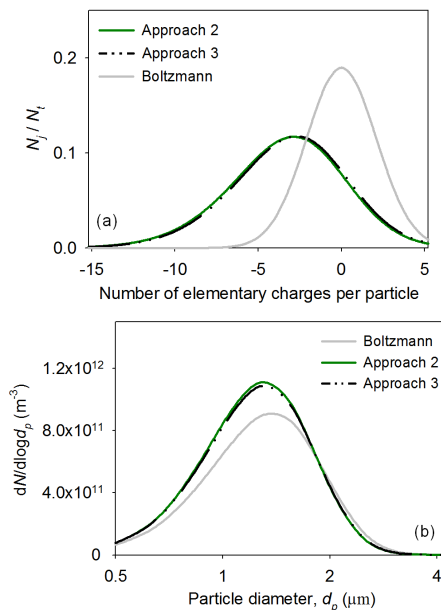


Figure 15. The charge (a) and size (b) distributions of initially monodispersed ^{134}Cs particles ($d_p = 0.5 \mu\text{m}$, $\eta_{\text{Cs-134}} = 14.5 \text{Bq}$; $N_t = 10^{13} \text{m}^{-3}$). The simulation time is 2 h.

Charging and coagulation of radioactive and nonradioactive particles

Y.-H. Kim et al.

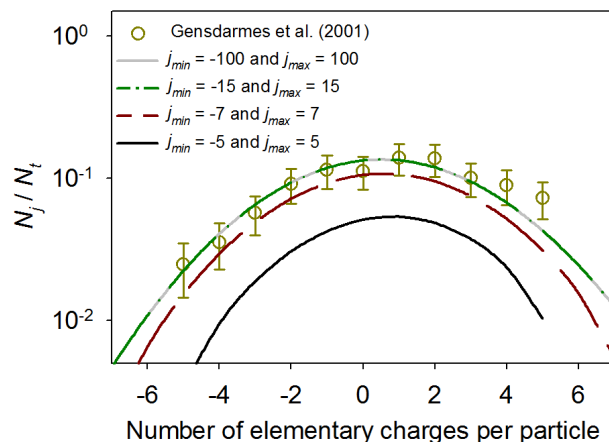


Figure 16. The charge distributions of monodispersed ^{137}Cs particles predicted under various boundary conditions ($d_p = 0.82 \mu\text{m}$, $\eta_{\text{Cs-137}} = 12.8 \text{ mBq}$, and $q_l = 7.1 \times 10^6 \text{ m}^{-3} \text{ s}^{-1}$). j_{min} and j_{max} represent the minimum and maximum values for particle charge classes.

Title Page

Abstract

Introduction

Conclusions

References

Tables

Figures

◀

▶

◀

▶

Back

Close

Full Screen / Esc

Printer-friendly Version

Interactive Discussion